

Solar Irradiance Variations: What have we learned from the past three solar cycles?

Lecture Notes for the Summer School in Alpbach 2010

Claus Fröhlich
Physikalisch-Meteorologisches Observatorium Davos
World Radiation Center, CH-7260 Davos-Dorf, Switzerland

1 Why do we need solar irradiance measurements from space?

The radiative output of the Sun was termed ‘Solar Constant’ until the start of solar monitoring by satellite experiments revealed that it varies continuously and exhibits variations on all time scales – from minutes to decades, accessed thus far. Prior to the advent of space-based observations, astronomers and solar physicists argued that the radiative output of the Sun as a star - the total solar irradiance (TSI) - changed in a substantial way only on evolutionary time scales of millions of years. While it was recognized that the occurrence of sunspots might change the irradiance at the Earth, their effect was considered negligible because they cover at most a few tenths of a percent of the visible solar disk. As well, the results of a half-century of ground-based program from 1902 to 1957 of the ‘solar constant’ by the Smithsonian Institution inferred changes associated with the Sun’s activity cycle for both the short-term decrease due to sunspots (Abbot, 1963) and the 11-year cycle, shown as a positive correlation between sunspot numbers and the solar constant especially during the strong solar cycle 19 (Abbot, 1952; Aldrich and Hoover, 1954). However, the determined amplitudes were nearly an order of magnitude higher than evident from the space-based record shown in Fig. 1. As a result, the view that the TSI was a constant quantity prevailed until the late 1970s, when space-based records became available. The first unequivocal evidence of TSI variability on time scales from minutes to days and months was published by Willson et al. (1981) from measurements by the ACRIM (Active Cavity Radiometer for Irradiance Monitoring) experiment on SSM (Solar Maximum Mission of NASA) during 1980 (see Fig. 1). The radiometer detected fluctuations that sometimes reached a few tenths of a percent and were associated with the movement of sunspots across the face of the solar disk visible at Earth as the Sun rotated on its axis. Such observations have been continued with overlapping missions until present and confirm TSI variability on all timescales. From these results it is clear that observations from space are needed, not only because of the stability of the space environment, but also because the extinction of the spectral radiation in the terrestrial atmosphere cannot be determined with sufficient accuracy to allow detailed and spectrally resolved corrections of ground-based TSI measurements. Even more important is the fact that the radiation below about 300 nm does not reach even the highest mountain tops and although this part contributes energetically only about 1%, its variability over a solar cycle is so high that about 20% of the variability of TSI comes from this part of the spectrum.

The understanding of these variations will not only improve the knowledge of the responsible mechanisms on the Sun, but also allow to reconstruct TSI back in time, possibly back to the Maunder Minimum in 17th century during which solar activity was very low with essentially no spots over a few decades and the temperature in Europe was low, it was the time of the so called ‘Little Ice Age’. Although the variability of spectral irradiance is very important especially in the UV and EUV range we will concentrate in this lecture on solar radiometry from space for the measurement of TSI. A review of the TSI variability can be found in Fröhlich and Lean (2004); Fröhlich (2009a,b).

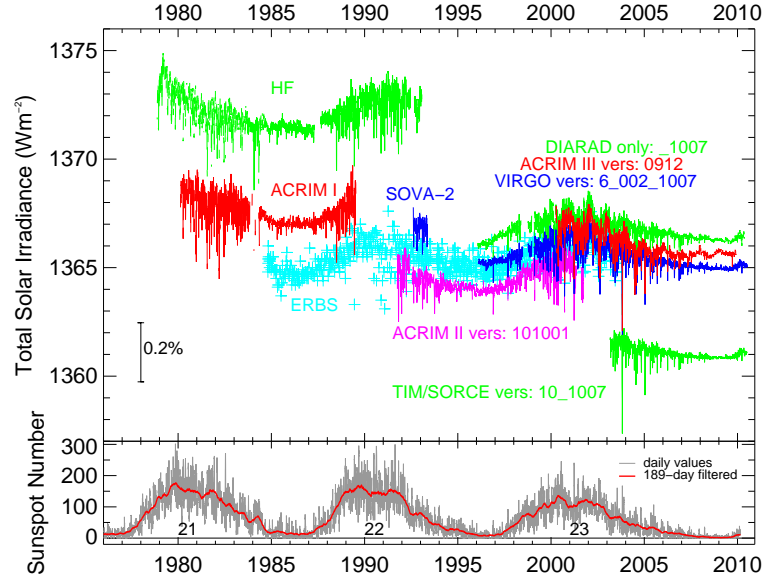


Figure 1: Top panel: Compared are daily averaged values of the Sun’s total irradiance from radiometers on different space platforms as published by the instrument teams since November 1978. Note, that the VIRGO TSI is determined from both VIRGO radiometers (PMO6V and DIARAD), whereas the DIARAD TSI is only based on this one alone. Bottom panel: Sunspot number to illustrate the variability of solar activity for cycles 21, 22 and 23.

2 Principles of solar radiometry, relative and absolute uncertainty

Solar radiometers are based on the conversion of radiation to thermal energy which is measured by an electrically calibrated thermal flux meter. Cavities are used to improve the absorption of solar radiation. They have an aperture, called a ‘precision’ aperture, which determines the flux-defining area, and a shutter, which opens and closes alternately while the thermal flux to the heat sink is maintained constant; this is called the active mode of operation, hence the name active cavity radiometer (ACR). Four types are currently used in space: ACRIM-III on *ACRIM-Sat* (Willson, 1979, 2001), PMO6V and DIARAD within VIRGO on *SOHO* (Brusa and Fröhlich, 1986; Crommelynck et al., 1987; Fröhlich et al., 1995, 1997) and TIM on *SORCE* (Kopp and Lawrence, 2005; Kopp et al., 2005). These references may be consulted for details of the construction of the radiometers, of their characterization and on how the uncertainties are determined. For a detailed discussion of the differences and similarities of the different approaches we refer to Fröhlich (2010a). We introduce the principle of solar radiometers with the PMO6V radiometer as an example. Figure 2 from Fröhlich et al. (1995) shows a cut through the radiometer and a block diagram of the control and measurement electronics. The front cavity is used to measure the radiation and the rear facing one is the compensating part of the differential heat flux meter; in this configuration the back cavity cannot be used for radiation measurements. In contrast DIARAD and TIM have all cavities side by side which allows radiation measurements with any of them alternatively. The active mode operation with a shutter open-closed cycle of 60 s/60 s is realized with the control circuit consisting of a Wheatstone bridge with the four wire-wound thermometers, a phase-sensitive detector (PSD) for the error signal, a proportional-integral (PI) control and a square-root circuit controlling the heater power in the front cavity. The value is set by the amount of power in the back cavity (REF). The electrical power in the front cavity is measured as voltage drop over the heater and a standard resistor.

As all classical radiometers the PMO6V is operated in a quasi-stationary mode with shutter cycles of 60 s. At the end of each phase the electrical power is read and the irradiance S evaluated according to

$$S = \frac{C}{A} (P_{\text{closed}} - P_{\text{open}}) \quad , \quad (1)$$

with A the area of the ‘precision’ aperture and C the total correction factor as determined by characterization which consists of the experimental determination of the deviations from the ideal behaviour under the conditions expected during a space mission (se e.g. Brusa and Fröhlich, 1986). The different effects considered are: reflectivity and efficiency of the cavity

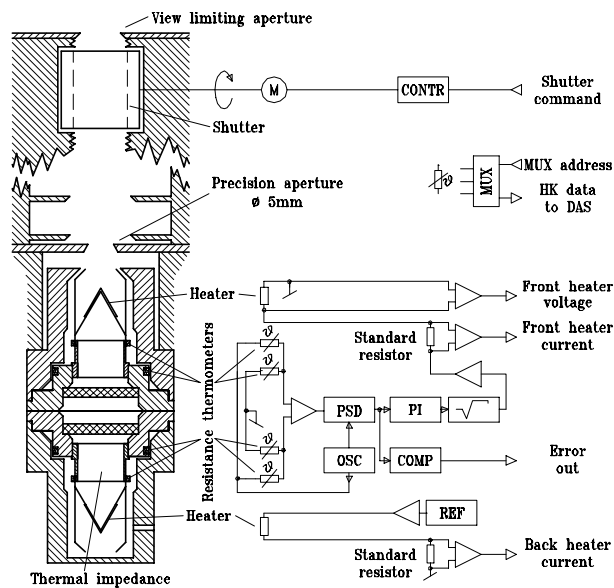


Figure 2: Schematic diagram of the PMO6V radiometer with its control electronics. The shutter behind the view limiting aperture is a drum which can be closed by turning it by 90° . The electronics control the active mode operation in which the heat flux (temperature difference across the thermal impedance of the front cavity) is maintained constant during the illuminated and reference phases. A picture of the radiometer is shown in Fig. 3.

absorption, the losses due to diffraction at the different apertures, stray-light in the muffler, heating of the leads (i.e. the connections of the heater) and the non-equivalence of the radiative and electrical heating. How well these deviations can be measured determines the uncertainty of the radiometer, which is of the order of $0.1 \dots 0.3\%$ for the classical radiometers. For TIM the uncertainty is of the order of 0.03% , this improvement is mainly due to the way it is operated (Kopp and Lawrence, 2005; Kopp et al., 2005). P_{closed} and P_{open} are the closed and open electrical power readings. This operation relies on a rather short time constant which is improved with the overall gain of the servo loop which is typically between three and five. So, an open-loop or natural $1/e$ time constant of about 20 s is reduced to 4 s to 7 s.

The value of TSI as determined from the above algorithms includes all known instrumental effects. It has to be normalized to 1 ua, the mean Sun-Earth distance, by multiplying the measured value by $(r_E/\text{ua})^2$, the actual value of the Sun-instrument distance being r_E . The relative correction varies between $\pm 3\%$ and can be done to a relative uncertainty of at least 1.0×10^{-7} from the ephemeris of the spacecraft. A further correction is needed for the Doppler effect due to the radial velocity between the source and the radiometer. The correction is proportional to $(1 - 2v_r/c_0)$ with v_r being positive away from the Sun. For a low-orbit satellite this correction can amount to up to $\pm 6 \times 10^{-5}$ with radial velocities of up to $\pm 9 \text{ km s}^{-1}$.

As stated before the absolute uncertainty of the classical radiometers is of the order of $0.1 \dots 0.3\%$. Figure 1 shows the improvement of characterization in the nineties resulting in a much closer agreement of the radiometers of different missions, now within about $\pm 0.1\%$ confirming the stated absolute accuracy. However, the results of TIM on SORCE showed results which are well outside the stated radiometric uncertainties. Investigations of this difference are ongoing, but a definitive explanation has not been found - it must, however, be an effect which is not included in the characterization of the classical radiometers with the possibility of aperture heating and/or stray light at the view-limiting aperture. These effects are avoided in TIM because the precision aperture is in front of the instrument and the view limiting is defined by the front area of the cavity.

Figure 3 shows the VIRGO sensor package with the instruments, which provides data since February 1996 from the ESA/NASA spacecraft SoHO - and hopefully continues into solar cycle 24 for another few years

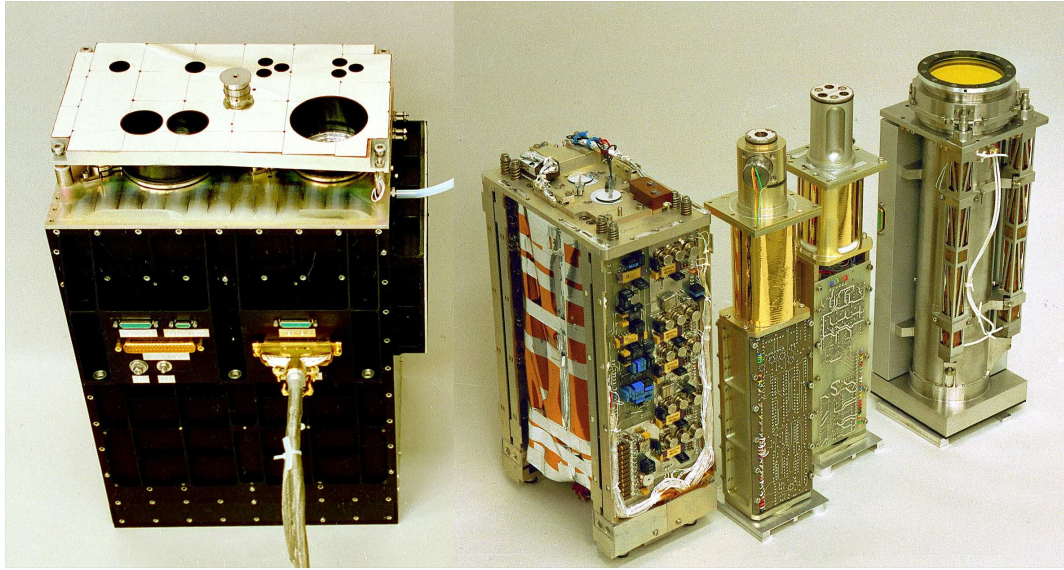


Figure 3: Left is the VIRGO sensor package (392x293x230 mm) and to the right the instruments: DIARAD, PMO6V, SPM and LOI.

3 Discussion of results from missions since 1978

3.1 Corrections for degradation and other long-term changes due to exposure to the Sun and the space environment

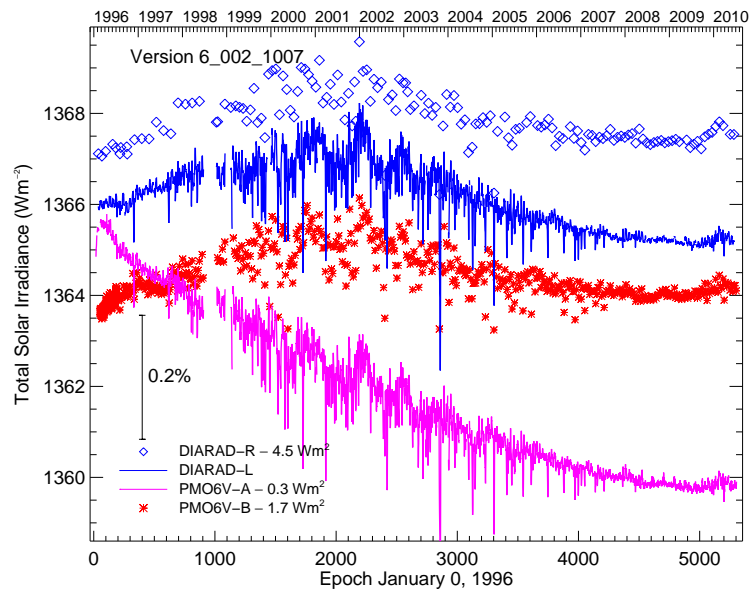


Figure 4: Level-1 data of the two radiometers on VIRGO: DIARAD-L and R and PMO6V-A and B. Note the difference in the amount of degradation of PMO6V-A relative to DIARAD-L and the early increase of the PMO6V-A and B.

From Figure 4 it is obvious that the long-term behaviours of the four VIRGO radiometers differ substantially from each other, and important corrections are needed to deduce a reliable TSI from these data. Already at this stage of the evaluation the different long-term behaviour of the operational PMO6V and DIARAD is very obvious. Also prominent is the early increase of the PMO6V radiometers during the first weeks of exposure. From the comparison of a back-up instrument

of the same type with much less exposure to solar radiation, changes due to exposure to the Sun can be determined. But these data are sparse and we need a reliable way to interpolate between the reference measurements in order to enable continuous correction of the operational radiometer. One may use fitting of polynomials of higher degrees (Willson and Hudson, 1991; Willson and Helizon, 2005) or one can use some other methods, e.g., running means (Dewitte et al., 2004a). A much better way is to use a model which also helps to understand the physical mechanisms. Such a model is based on a hyperbolic function (e.g., Fröhlich and Anklin, 2000; Fröhlich and Finsterle, 2001; Fröhlich, 2006) which is the solution of the differential equation describing the ‘siliconizing’ of a quartz window exposed to UV radiation, that is, a change of the optical properties due to the formation of silicon at the surface with a subsequent decrease of the response of the underlying quartz to radiation exposure. The ‘siliconizing’ is an example for a physical effect which may be underlying degradation of optical surfaces as e.g. black paints, metallic surfaces, filters. The time-dependent sensitivity change $\Delta S(t)$ can be described with t_{exp} for the exposure time and $d(t)$ for the dose-corrected exposure time

$$d(t) = \int_0^{t_{\text{exp}}} (\lambda m(t) + 1) dt \quad (2)$$

as a hyperbolic function

$$\Delta S(t) = a \left[\left(1 + \frac{1}{b \tau_C} d(t) \right)^{-b} - 1 \right] \quad (3)$$

with a , λ , b and $1/(b \tau_C)$ as adjustable parameters. The parameter b has been included in τ_C , which then corresponds to a 1/e time constant. This hyperbolic function transforms into an exponential function for large b as

$$\Delta S(t) = a \left[\exp\left(-\frac{1}{\tau_C} d(t)\right) - 1 \right]. \quad (4)$$

For $b < 20$ the differences in the determined parameters are substantial, although the goodness of the fit with both functions is similar. So, in the analysis one can use Eq. 4, but may need to check with a fit according Eq. 3 the size of b in order to properly identify the physical meaning of the coefficients. The dose $m(t)$ in $d(t)$ is deduced from the MgII index as surrogate for the UV radiation, normalized to $-0.5 \dots + 0.5$. The fitted parameter λ provides the information about the wavelength responsible for the effect as it is related to the cycle variability of the corresponding wavelength. The normalized MgII index $m(t)$ is shown in Fig. 5 for the last three solar cycles. This analysis not only explains the dose

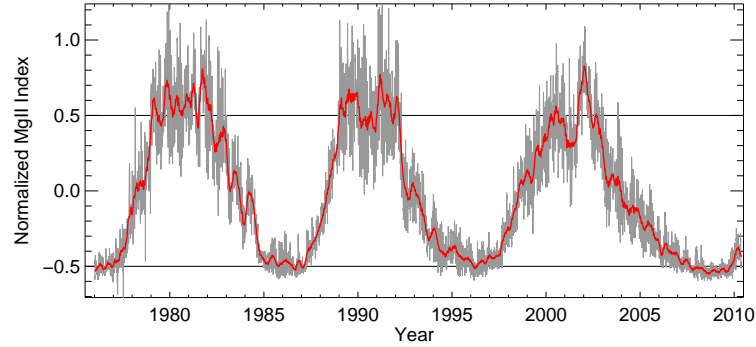


Figure 5: Time-series $m(t)$ of the normalized MgII index as proxy for solar UV irradiance determining the dose. The MgII index is a core-to-wing ratio of the MgII h and k lines around 280 nm.

dependence of the changes, but also provides information about the physical mechanisms behind it (for details see also Fröhlich, 2010c).

During a recent re-analysis of the VIRGO SPM it became clear (see Fig. 6) that the degradation also depends on the prevailing temperature via a Boltzmann factor $\exp(-\frac{E}{kT})$. Linearized around the mean temperature T_0 this factor can be expressed as $\exp(-\frac{E}{kT_0})(1 + \frac{E}{kT_0} \Delta T)$ with $\Delta T = (T - T_0)/T_0$. Thus, the dose dependent exposure time $d(t)$ becomes

$$d(t) = \int_0^{t_{\text{exp}}} ((\lambda + \alpha \Delta T)m(t) + 1) dt. \quad (5)$$

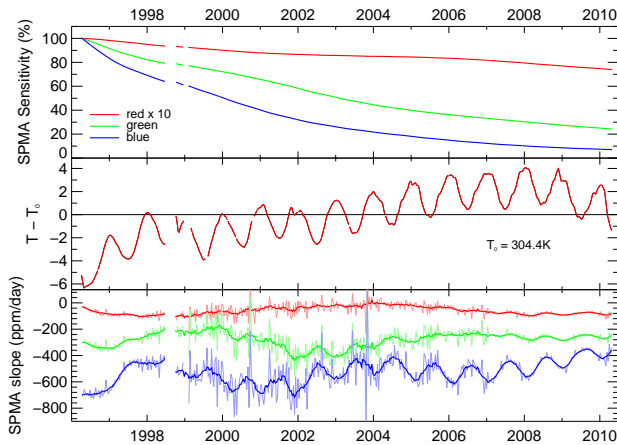


Figure 6: Top panel: Sensitivity change of the three operational VIRGO/SPM. Middle panel: Temperature of the operational VIRGO/SPM. Bottom Panel: Slope of the sensitivity change in ppm/day which obviously depends not only on the dose, but also on temperature. Note that higher temperatures result in steeper slope.

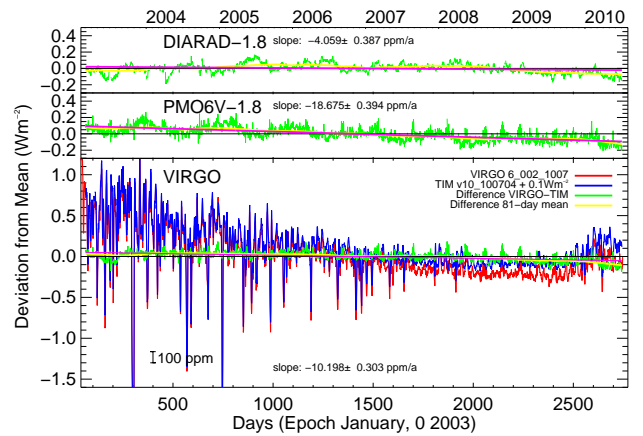


Figure 7: Top panel: Comparison of the DIARAD Level 1.8 with TIM on SORCE. Middle panel: Comparison of the PMO6V Level 1.8 with TIM. Bottom Panel: Comparison of the final VIRGO TSI with TIM on SORCE.

In the case of VIRGO this analysis works well for the PMO6V radiometers, whereas the changes of DIARAD are a mixture of exposure-dependent and also non-exposure-dependent changes which makes such an analysis difficult (for details see e.g. Fröhlich, 2003). In the present analysis of the VIRGO radiometers this temperature dependence has not yet been included, but it may explain the annual cycle variations observed in the comparison of the PMO6V and TIM data as illustrated in Fig. 7 - a corresponding re-analysis is planned for the near future.

As an illustration of the method, the behaviour of ACRIM-I is shown in Figure 8 and indeed the hyperbolic function explains the behaviour of the degradation changes quite well. It shows also how important the dose is, and that neither the exposure time alone nor a simple polynomial fit is sufficient — especially if the activity level is changing during the period analysed.

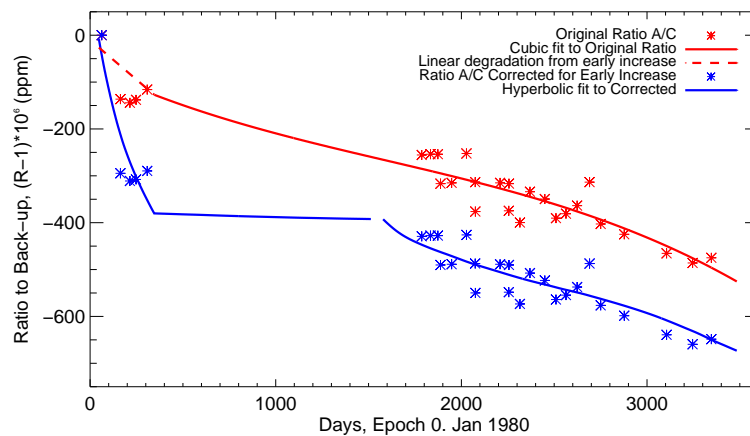


Figure 8: The original ratios of sensor A to sensor C (red symbols) of the ACRIM-I experiment on *SMM* are from Willson and Hudson (1991). The cubic fit corresponds to the correction originally applied and the dashed line includes the linear fit found by fitting the early increase (not shown). The blue symbols are corrected for the early increase (see Fig. 2 of Fröhlich, 2006). and then fitted with a hyperbolic function. Note the dose-dependent change over the period of the spin mode (days 300-1600 on the time axis) and after the solar minimum of 1986 (after day 2100). Adapted from Fig. 3 of Fröhlich (2006).

3.2 Construction of a consistent TSI composite

The time series of the HF, ACRIM I, II and III and VIRGO radiometers as shown in Fig. 1 can be used for the construction of a TSI composite by shifting each series to a common level and merging them together. Presently there are three composites available, the first one was presented in 1997 at the IAU General Assembly in Kyoto by Fröhlich and Lean (1998a) and is now called PMOD composite (for its construction see Fröhlich, 2006). A few months later the ACRIM composite was published by Willson (1997) which has been updated in 2003 by Willson and Mordvinov (2003). Somewhat later a third composite, called IRMB, was presented by Dewitte et al. (2004b). These composites are available from the corresponding teams ¹. The ACRIM and IRMB composite use the data as published, whereas the PMOD composite introduces corrections of effects not considered in the original data analysis. Already in the early versions of the PMOD composite corrections for the HF degradation were applied (Fröhlich and Lean, 1998a,b). Similarly, the degradation of ACRIM-I during first years was corrected for the effect of the rather short exposure time during the spin mode which was not taken into account in the original treatment by Willson and Hudson (1991). The corrected HF time series was used for the period before ACRIM started and during the spin mode of SMM and the corrected ACRIM I for the rest of time (1980 and 1984–1989) as basis for the composite of Fröhlich and Lean (1998b). Fröhlich (2006) included a further correction of ACRIM I for the early increase which was first observed in the PMO6V measurements of VIRGO/SOHO and seems to be an inherent effect of most classical radiometers. Moreover, the substantially lower exposure time during the spin mode operation of SMM 1981–1984 imposed to take the effective dose into account which changes the rate of degradation substantially (see Fig. 3 and 4 of Fröhlich, 2006). During the first 15-months of HF no other radiometer is available as reference and a proxy model was used. This is the only period when a model is involved as reference. It is, however, calibrated to the corrected ACRIM I data over the period from 1980–1988 and is thus quite reliable for the period of a few years before 1980. For HF all glitches throughout the mission are removed first and then the corrections for the early increase, the degradation and the long-term sensitivity increase were determined over the full period from November 1978 until January 1993, which yields an internally consistent time series (see Fig. 6 and 7 of Fröhlich, 2006).

Another problem for the composite constructions is how to bridge the so-called ACRIM gap between the end of ACRIM-I and the start of ACRIM-II (June 1989 to October 1991). During this period daily values from HF and some 70 data points from ERBE with a sampling every 14 days are available. Already Lee III et al. (1995) revealed two slips in the HF data resulting in a total change of -0.68 Wm^{-2} over this period which was confirmed by comparison with a model derived from solar disk observations by the San Fernando group (Chapman et al., 1996). Fröhlich (2000) re-analyzed this period and the overall change was again confirmed, but with a slightly different value of -0.58 Wm^{-2} . Such changes no longer need to be corrected individually, because the HF time series, consistently corrected over its full period of observation, can now be used directly for bridging the ACRIM gap.

The ERBE data set covers the period from 1985–2003 and more specifically the controversial time of the ACRIM gap. Although the record is quite noisy – mainly because of a low rate of sampling every 14 days – it can be used to illustrate the differences between the three composites as shown in Fig.10. The ACRIM composite neglects the corrections of the HF during the ACRIM gap and thus shows a significant upward trend of TSI between 1985 and 1995 (Willson, 1997; Willson and Mordvinov, 2003; Scafetta and Willson, 2009). The IRMB composite traces ACRIM II to I via ERBE which results in an insignificant difference between the two minima in 1985 and 1995 similar to the PMOD composite. However, the IRMB times series during the ACRIM gap shows a strange variation which comes from the fact that it is normalized to the average of ERBE and HF referred to the SARR reference (SARR: Space Absolute Radiometric Reference as defined by Crommelynck et al. (1995)). During the period of SOHO the IRMB composite is based on DIARAD data alone, which means that it is corrected for degradation by comparison with its back-up, but misses the effect of non-exposure dependent sensitivity increase. This latter effect can only be determined by comparison with another radiometer - in the case of VIRGO with PMO6V - and its omission is the main reason for the increase of TSI during solar cycle 23 in contrast to the PMOD and ACRIM composites (see also Fig. 10). The deviation from ERBE can be fitted with an exponential function similar to the one which is used in the evaluation of the VIRGO data to correct DIARAD for the non-exposure dependent changes (Fröhlich, 2003). Furthermore, both the ACRIM and IRMB composite use the original data for the early part of the NIMBUS-7 mission which is - as explained above - strongly influenced by instrumental changes and is not representing solar variability.

¹PMOD: <http://www.pmodwrc.ch/pmod.php?topic=tsi/composite/SolarConstant>, ACRIM: <http://www.acrim.com/Data%20Products.htm> and IRMB: <http://remotesensing.oma.be/en/3377935-TSI+composite.html>

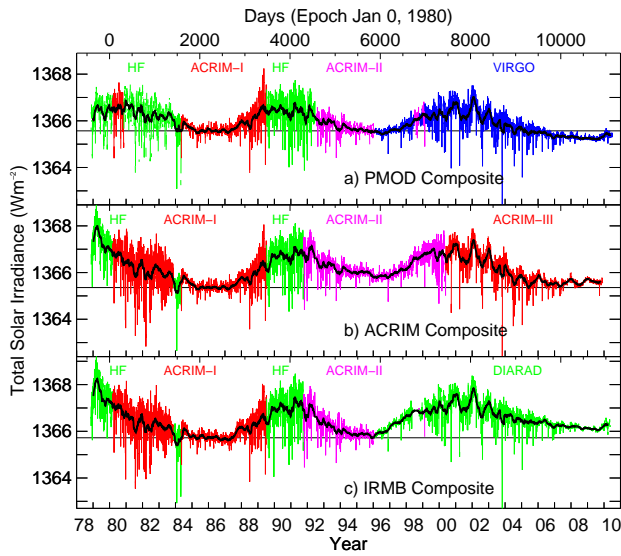


Figure 9: Shown are the three composites: a) PMOD (Fröhlich and Lean, 1998a; Fröhlich, 2006), b) ACRIM (Willson, 1997; Willson and Mordvinov, 2003) and c) IRMB (Dewitte et al., 2004b).

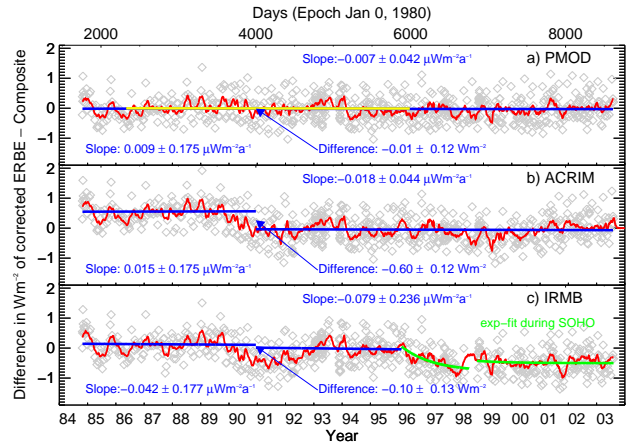


Figure 10: Shown are comparison of the three composites with the 18-years record of ERBS from 1985 – 2003: a) PMOD (Fröhlich and Lean, 1998a; Fröhlich, 2006), b) ACRIM (Willson, 1997; Willson and Mordvinov, 2003) and c) IRMB (Dewitte et al., 2004b). The yellow line in a) is the result of the linear fit to the difference over solar cycle 23.

Recently Scafetta and Willson (2009) and Scafetta (2010) insinuated again that the PMOD composite is incorrect, because the corrections applied to the original ACRIM I and HF time series have no basis at all and are only applied to get agreement with a proxy model originally proposed by Foukal and Lean (1988, 1990). As explained in detail in Fröhlich (2006) and summarized above, the corrections are based on an improved understanding of the long-term behaviour of radiometers in space the results of which was not available to the teams evaluating ACRIM and HF. This was made possible by the detailed analysis of the almost 14-years long solar irradiance record from the two VIRGO radiometers (PMO6V and DIARAD) on a thermally very quiet spacecraft SOHO (see e.g. Fröhlich, 2003, and references therein). Besides the excellent agreement with the ERBE record the PMOD composite agrees also much better with proxy (e.g. Fröhlich and Lean, 2004; Fröhlich, 2009a) and other models Wenzler (2005); Wenzler et al. (2009); Krivova et al. (2009), which demonstrates the consistency of the applied corrections. Thus, the PMOD composite is a reliable representation of TSI back to November 1978. From the experience gained by extrapolating ACRIM I back to the beginning of HF the PMOD composite can be further extended back to the beginning of 1976 in order to cover cycle 21 from its minimum in 1975 as shown in Fig. 11.

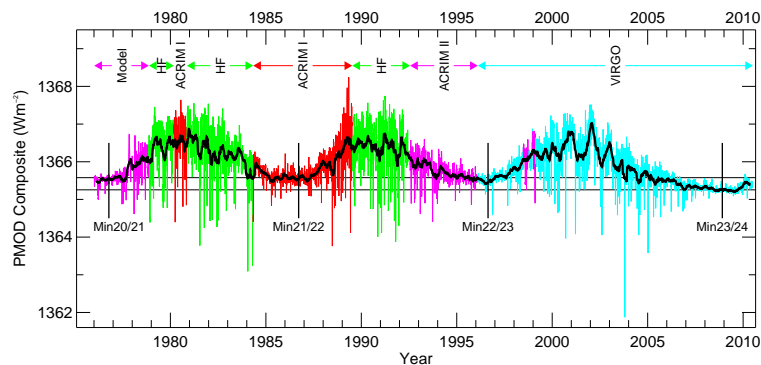


Figure 11: Daily TSI of the PMOD composite (updated until end of March 2010, Version 41_62_1003a) and extrapolated with a proxy model back to 1976. The amplitudes of the three cycles decrease first and then increase again. The two horizontal lines indicate the value of the minima in 1986 and 2008, respectively. Note the low value of the 2008/9 minimum, which is 0.22 Wm^{-2} lower than the previous one, or 25% in terms of the mean cycle amplitude.

4 Solar Irradiance Variability

4.1 What is the origin of the Variability of Solar Irradiance?

Figure 11 shows clearly that the TSI is variable on all time scales from days to decades. There are obvious changes on the solar rotation (27-day) timescale during the passage of active regions with dips due to sunspots and rises due to faculae. Moreover, there is also a modulation with the 11-year period which may change in amplitude from cycle to cycle. The fact that TSI is higher during high activity contradicts the conjecture that more sunspots should make a darker sun, but it supports the solar-terrestrial relationship that low TSI may lower the Earth's temperature as during the little ice age in Europe in the 17th century when the sun showed very low activity with essentially no visible sunspots, a coincidence first noted by Eddy (1976), who called this grand minimum 'Maunder Minimum'. During the most recent cycle the number of sunspots was less than during the two cycles before (see lower panel of Fig. 1) and there were even periods with essentially no spots which made the TSI amplitude during this cycle of the same order as during the ones before. The amplitude is defined here as an equivalent of a sine square (twice the average between the minima of the considered quantity). This may not ideally represent the detailed behaviour of a solar cycle, which shows a much faster increase during the ascending phase compared to the rather slow decrease during the descending phase (see e.g. Fig. 11). Besides the fact that this definition can be applied to any other quantity considered, it is for TSI relevant for the solar-terrestrial influence on the global climate with its rather long response time. Also an independent definition of the 'time of minimum' is needed and the first appearance of an important sunspot group of the new cycle (at high latitude and of opposite polarity) is used. The dates of the last four minima are 10 October 1976, 19 September 1986, 21 August 1996 and 29 November 2008.

Solar activity is driven by the magnetic fields produced periodically by a dynamo at the base of the convection zone at about $0.71R_{\odot}$ (for a review see e.g. Charbonneau, 2005, and references therein). Magnetic fields threading the visible solar surface, the photosphere, produce features like sunspots and faculae related to active regions and bright network in and outside active regions. Figure 12 shows time series for solar cycles 20–23 of typical measures of solar activity. The sunspot number (SSN, Fig. 12a) is certainly the most widely used index mainly because it is available since the 17th century, but also because its cycle amplitude represents a measure for the varying amount of bipolar regions reaching the surface and hence the strength of solar activity during a cycle. The next parameter is the solar radio flux at 10.7 cm (F10.7, Fig. 12b) which is an absolute physical measurement available since 1947 (solar flux units $\equiv 10^{-22} \text{ W m}^{-2} \text{ Hz}^{-1}$) which similar to the SSN represents a measure of the strength of solar activity. Figure 12c shows daily values of the Ly- α composite (starting with the measurements by AE-E from Woods et al. (2000)) which is representative to the changes in solar chromosphere due to the magnetic fields on the surface. A similar behaviour show the CaII K and MgII indices (Fig. 12d and e) which also represent changes of the chromosphere due to the surface magnetism. None of these quantities show a significant decrease during the recent minimum as TSI. The observed trends between minima are at least a factor of 5–6 smaller than for TSI as summarized in Table 1.

For SSN, such a behaviour is expected as the number cannot be negative, but all the other parameters of Fig. 12 have no lower limit of their values and thus could show a similar change as TSI. For F10.7, there is no significant change of the values at minima back to the start of the measurements in 1947. The CaII K index deduced from the Mt Wilson and Kodaikanal observations (Foukal et al., 2009) back to around 1910 shows also no change in the minima to within $\pm 4\%$. As the chromospheric indices are highly correlated with the UV and EUV irradiance and as shown by the Ly- α record, secular changes of the spectral irradiance below about 300 nm are hence unlikely. All these observations show that the chromospheric temperatures during minima and hence the 'quiet' magnetic Sun does not seem to change on secular timescales (see also Livingston and Wallace, 2003). This observation contradicts the assumption that the long-term changes of solar irradiance – spectral or total – are caused by the same mechanism as the intra-cycle variation, namely by manifestations of the surface magnetic fields, that is sunspots, faculae and network, including ephemeral regions (for a description see e.g. Harvey, 2000).

As shown in Fig. 13 and Table 1 the only parameter that does exhibit inter-cycle changes similar to TSI is the open magnetic field, B_R , as observed at 1 AU by satellites since the sixties (Fig. 13b). B_R is determined by taking the absolute value of the daily mean of B_X from the OMNI2 dataset². Recently, Lockwood et al. (2009a,b) have shown that a kinematic correction is needed to determine the open field of the sun at the source region (at $2.5 R_{\odot}$) from the measurements at 1 AU. This

²available from ftp://nssdcftp.gsfc.nasa.gov/spacecraft_data/omni/omni_m_daily.dat

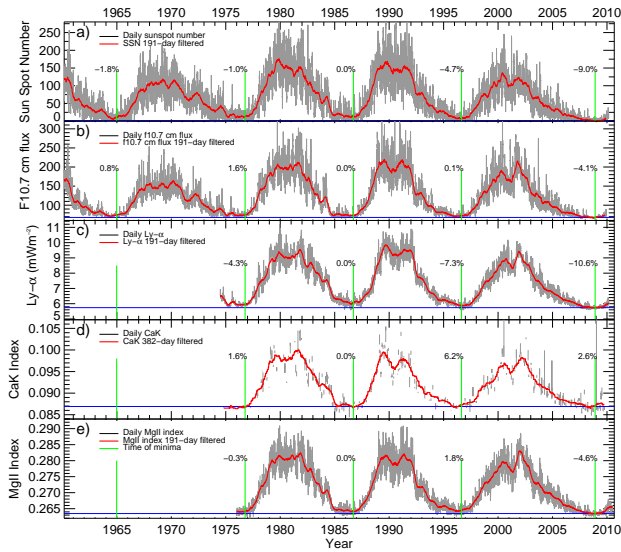


Figure 12: Daily values of the time series of a) SSN, b) F10.7, c) Ly- α irradiance, d) CaIIK and e) MgII indices. The values indicated at solar minima (above the vertical lines) are the percent changes relative to the amplitude of cycle 22 and normalized to the value between cycles 21 and 22 indicated by the horizontal blue line. In contrast to TSI of Fig. 11, none of these records show the large decrease during the present minimum.

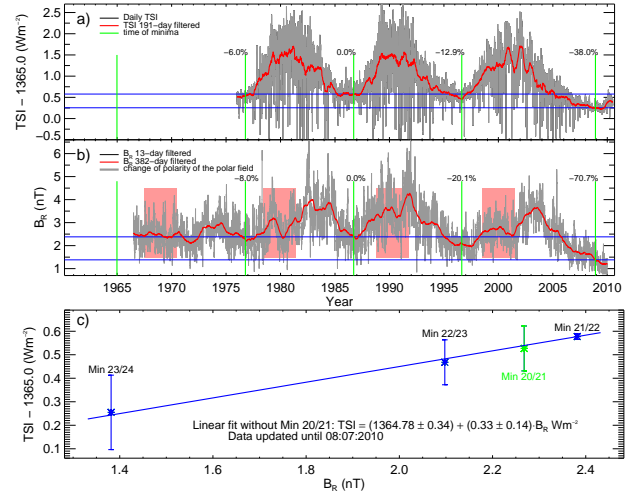


Figure 13: Comparison of TSI and the open solar magnetic field. a) daily values of TSI (as Fig. 1) and b) those of the open magnetic field B_R at 1 AU. The correlation between the minimum values of TSI and those of B_R (blue points and the blue line) is shown on c). The green point is the extrapolated value not used in the regression. The error bars are from a detailed analysis as described in Fröhlich (2009b) and the errors of regression coefficients include these uncertainties, and hence are quite large.

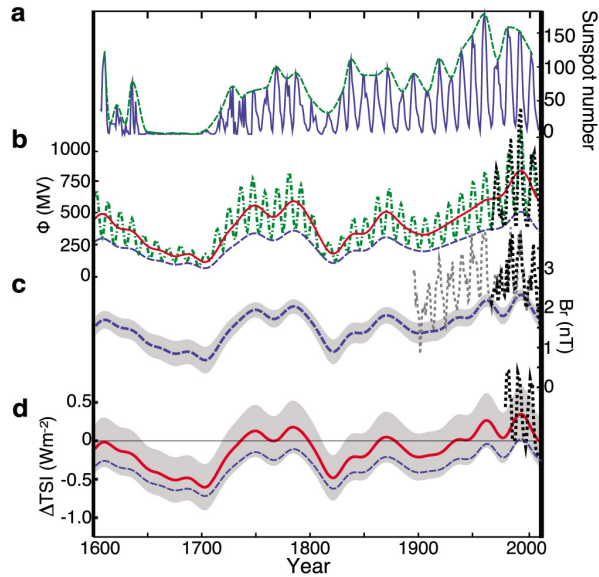


Figure 14: Data since 1600 up to present. (a) Group sunspot number. The full line are annual values, and the dashed line is the envelope going through the 11-year solar cycle maxima. (b) Solar modulation potential Φ . The full line shows 40-year averages of Φ as derived from ^{10}Be (Steinhilber et al., 2008). The dash-dotted line is Φ extended with estimated 11-year solar cycle variations. The dashed line is the lower envelope. Black dotted are annual averages of Φ from neutron monitor count rates. (c) Open solar magnetic field B_R . The dashed line is B_R during the 11-year solar cycle minima derived from Φ (according to Eq.3 of Steinhilber et al., 2009) with the shaded band showing the estimated uncertainty. Dotted are annual averages of B_R (back to 1963) from the OMNI dataset and of the reconstruction of Rouillard et al. (2007) (back to 1895). (d) TSI relative to the value of the PMOD composite during the solar cycle minimum of the year 1986 (1365.57 Wm^{-2}). The dashed line is TSI during the 11-year solar cycle minima and the full line is solar cycle averaged TSI. Black dotted are annual averages of the PMOD composite.

Table 1: Cycle amplitudes and relative changes of minima in percent of the amplitude during cycle 22. The amplitudes are equivalent sine-squared with the trend during each cycle removed. The units are: TSI (Wm^{-2}), the open field at 1 AU B_R (nT), SSN (number), F10.7 ($\text{sfu} \equiv 10^{-22} \text{Wm}^{-2}\text{Hz}^{-1}$), Ly- α (mWm^{-2}), CaII K and MgII indices (core-to-wing ratio). Updated from Fröhlich (2009b).

Parameter	Cycle 20	Cycle 21	Cycle 22	Cycle 23
corrected cycle amplitude				
TSI	...	0.9244	0.8489	0.8427
B_R	...	1.361	1.482	1.161
SSN	95.1	139.8	132.9	98.1
F10.7	76.7	125.5	121.3	94.3
Ly- α	...	3.48	3.15	2.63
CaII K	...	0.01270	0.00992	0.00810
MgII	...	0.0175	0.0151	0.0137
change of minima over each cycle in percent				
TSI	...	6.0	-12.9	-25.0
B_R	...	5.0	-17.4	-45.8
SSN	0.8	1.0	-4.7	-4.3
F10.7	0.8	-1.6	0.1	-4.0
Ly- α	...	4.3	-7.3	-3.4
CaII K	...	-1.6	-2.7	-1.5
MgII	...	0.3	1.8	-2.8

correction, however, is not needed because B_R as defined here is more directly related to the interplanetary field (IMF) than the true open field and the IMF is what can be inferred from e.g. the concentration of cosmogenic isotopes in ice cores produced by the galactic cosmic rays (GCR) or from magnetic measurements on Earth like the aa index. B_R has an intra-cycle variation quite different from TSI, because B_R changes sign around the maximum of the cycle (during periods of the redish areas in Fig. 13b), and since the northern and southern hemisphere may change at different times, it is a prolonged period during which the behaviour of the B_R variability is dominated by this reversal. This reversal happens during each cycle and produces the 22-year magnetic Hale cycle with the solar polar field having the same polarity as Earth's field. B_R during minima is mainly determined by the polar field of the sun and thus is more representative of the strength of activity during the solar cycle before and after than to the amount of surface magnetism which is mainly determined by the non-axisymmetric fields.

Figure 13c shows the correlation between TSI and B_R as determined by linear regression. It is interesting that the line is very close to the points - much closer that one would expect from the error bars. This is also true for the point of the 1976 minimum, which is not used in the regression, indicating that its value - although based on a proxy model - is indeed quite reliable. The result of this correlation can be now used to calculate TSI at minima whenever B_R is known. An example of such a reconstruction of TSI during the Holocene is based on the record of the cosmogenic isotope ^{10}Be and shown in Fig. 14 back to the Mounder minimum in the 17th century (from Fig. 1 of Steinhilber et al., 2009). It is important to note, that this correlation does not mean a direct physical relationship between TSI and B_R . As already suggested by Tapping et al. (2007) and Fröhlich (2009b) the long-term trend may be due to global temperature change of the Sun with a magnitude related to the strength of the activity and hence to B_R during minima. The temperature change needed to explain the difference between the last two minimums is of the order of 0.25 K.

4.2 Proxy model based on four components

Proxy models of TSI are based on daily indices representing the darkening of sunspots and the brightening by faculae and network as illustrated in Figure 15. A 2-component model uses information on sunspots, ΔS_S from daily observations of their position and area, and one index for the brightening features ΔS_F , from e.g. MgII index. A 3-component model uses two different indices for the brightening, ΔS_F and ΔS_N (for a review see e.g. Fröhlich and Lean, 2004, and references therein). But, as all three components do not show substantial changes between minima a fourth component is needed

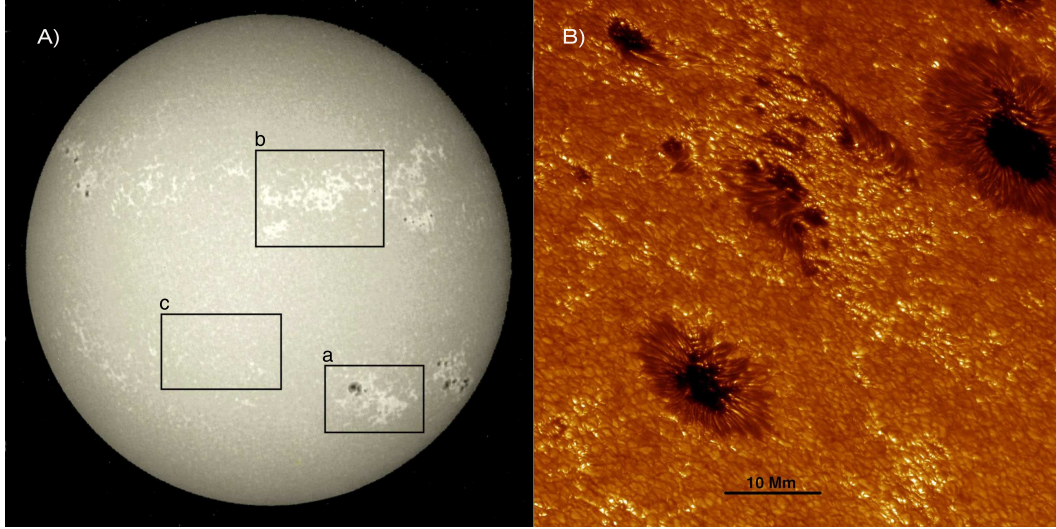


Figure 15: A) Sunspots and faculae in active regions (a,b), and network (c) imaged in the chromospheric CaII K line where faculae and network are enhanced over their contrast in broad-band light and seen as so called plages and bright network (image taken by the National Solar Observatory on 28 Aug 1988). B) A detailed image of the active region on the left limb as seen in the g-band (430.5 nm). The granules, covering most of the area, are the convective flows transporting the energy from the interior which contribute the steady component of the solar radiation. The magnetic features in an active region are the sunspots with the dark umbra and somewhat brighter penumbra and the faculae which are a dense carpet of bright points. (Image taken with the Swedish 1-m Solar Telescope by Dan Kiselman on 29 June 2003)

to model the trends of TSI between the minima as already shown by Fröhlich (2009a). The fourth component can now be constructed from the values of B_R at the minima, connected by linear trends and providing ΔS_T . Since sunspots and faculae typically occur on the Sun together, a competition of their relative strengths determines the short-term solar irradiance variability. The solar cycle amplitude seem to be determined by magnetic features with smaller sizes than sunspots and faculae and distributed all over the sun as network and the small bipolar Ephemeral Regions (see e.g. Harvey, 1994). The part coming from the latter are in the following included in what is called network. So, the 4-component proxy model model of TSI can be constructed as

$$S(t) = S_Q + a_F P_F(t) + a_N P_N(t) + a_S P_S(t) + a_T P_T(t), \quad (6)$$

with the value of the quiet Sun, S_Q , and $a_{F,N,S,T}$ the four coefficients for the influence of faculae, network, sunspots and the trend from ΔS_T .

Sunspot darkening, the fractional change in TSI caused by sunspots, is calculated explicitly as

$$P_S = \sum \Delta S / S_Q = \sum \mu A_s \alpha_s \frac{R(\mu)}{\int_0^1 R(\mu) \mu d\mu} \quad (7)$$

where ΔS is the reduction in irradiance relative to the quiet Sun, S_Q , for a sunspot of area A_s (in fractions of the solar hemisphere) at location μ in heliocentric coordinates. $R(\mu)$ is the center-to-limb variation function which is assumed to be the same for the quiet photosphere and the spot and α_s is the bolometric contrast. The summation is over all spots on the solar disk at a specific time, and utilizes bolometric contrast and center-to-limb functions (Eddington limb darkening $R(\mu) = (3\mu + 2)/5$) or more elaborate functions of μ as e.g. from Pierce (2nd edition, 2000)) appropriate for modelling total or also spectral solar irradiance variations. Ground-based white light images made from 1882 to 1976 by the Greenwich Observatory, and most recently by the U.S. Air Force at the operational Solar Observation Optical Network (SOON) sites. Observations of the sunspot regions are available from the National Geophysical Data Center (NGDC) operated by the National Oceanographic and Atmospheric Administration (NOAA) at Boulder, Colorado³, and supply the basic time-dependent information about sunspot areas and locations. Greenwich sunspot areas are reported to be 20-40 %

³ftp://ftp.ngdc.noaa.gov/STP/SOLAR_DATA/SUNSPOT_REGIONS

larger than SOON sunspot areas (Fligge and Solanki, 1997; Balmaceda et al., 2009). The differences between these two datasets were determined by Balmaceda et al. (2009) and have been confirmed for the period after January 1977 when the SOON data started (Fröhlich, 2010b). Hence they are corrected to agree with the Greenwich data, mainly to get a consistent record for the period from 1882 until present.

The sunspot data from January 1975 – February 2010 are used to determine P_S together with a contrast function which depends on the size of the spot as determined by Steinegger et al. (1990) and later Steinegger et al. (1996). The results are shown in Fig. 16a (on the plots P_S is identified as PSI, and they are given in parts per million, ppm).

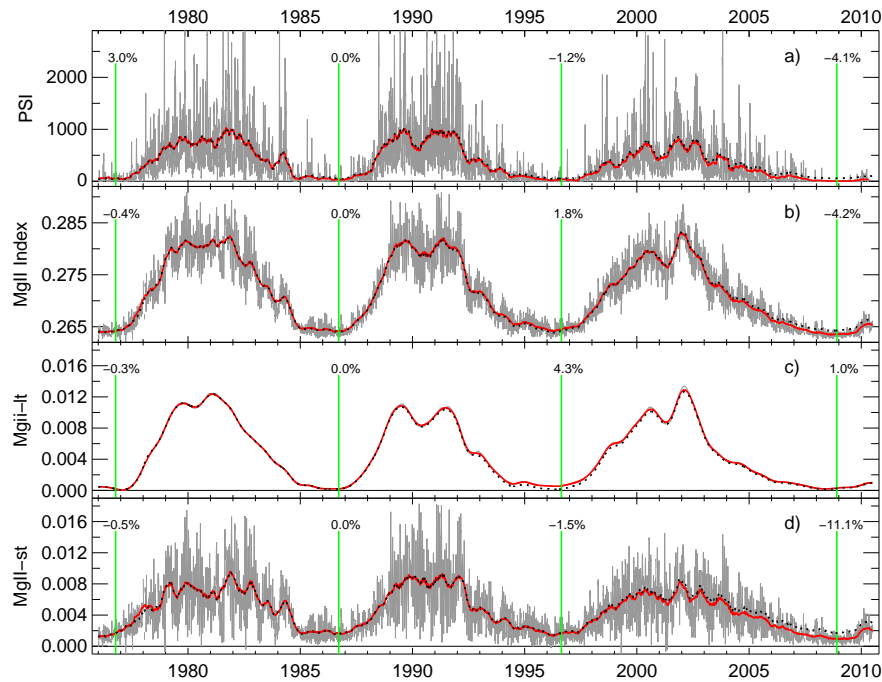


Figure 16: Daily PSI (a), MgII index as observed (b) and decomposed in a long- (MgII-lt: c) and short-term (MgII-st: d) part. Times of the minima are given as vertical green lines and are labelled with the percentage deviation of that minimum from the value of the minimum around 1986 relative to the mean amplitude of the parameter. The dotted lines correspond to the parameter if a linear trend between minima is removed.

Images like Fig. 15A can provide areas covered by plages and bright network in the upper solar atmosphere which in turn can be used to determine the effect of photospheric faculae and network on TSI. Such images are called spectroheliograms because they are observed in a narrow wavelength band in the resonance line of CaII K at 393.37 nm, which is the strongest solar spectral line observable from the ground. Archives of daily spectroheliograms maintained at Kodaikanal Observatory (KKO), India, since 1907 and at Mt. Willson Observatory (MWO), USA, since 1915 provide the longest available record of the daily changing structure of magnetic plages and network (see e.g. Foukal et al., 2009, and references therein). Spectroheliograms compiled since 1965 (as Fig. 15A) at the National Solar Observatory (NSO) provide supplementary information. The MWO record was discontinued in 1985 and the ones of KKO and NSO in 1999. These spectroheliograms can be analysed individually to determine the area and position of the faculae and bright points (Foukal et al., 2009; Tlatov et al., 2009; Ermolli et al., 2009), as it is done from images in magnetograms for the SATIRE model (e.g., Unruh et al., 2000; Krivova et al., 2003).

At Kitt-Peak Observatory monthly observations of disk-integrated CaII K-line fluxes started in 1975 and proved to be a good surrogate for the plage and network area covering the Sun. With the start of NIMBUS7 observations of the core-to-wing ratio of the MgII H & K lines, called MgII index (Heath and Schlesinger, 1986), became available. Now there is a continuous daily record since November 1978, which is updated weekly with SOLSTICE/SORCE data (Viereck and Snow, 2008). The time series of the MgII index used here is shown in Fig. 16b and is separated into a short- and long-term part, MgII-st and MgII-lt. This separation is performed by calculating a running average of the standard deviation over 217 days (8 solar rotations) which is then used - multiplied by an appropriate factor - to define the lower limit of the

short-term variations of the MgII index. The values above this limit is the short-term part of Fig. 16d and the values below the long-term part of Fig. 16c. The reason for calling the short-term part the facular contribution is quite clear - it is related to the passage of active regions on rotational timescale. As shown below, the long-term part gets a much higher coefficient from the multi-linear regression analysis. This can be interpreted as coming from small magnetic features, called here the network, which have a higher specific contrast for TSI than larger ones as found by Ortiz (2005) from MDI data. So the daily MgII-lt values are used for $P_N(t)$ and those of MgII-st $P_F(t)$ in Eq. 6, providing the second and third component of the proxy model. Figure 16c and d illustrate the influence of faculae and network during the recent minimum and show that its value is determined by the small number of faculae of faculae and not by the network. This is further support of the fact that the chromospheric indices do not show a secular trend and confirming the conclusions of a recent study of the long-term behaviour of solar like stars by Judge and Saar (2007).

The value of the quiet Sun, S_Q and coefficients $a_{F,N,S,T}$ are determined by a multi-linear regression according to Eq. 6 with the extended PMOD composite for $S(t)$. The results are shown in Table 2 and Fig. 17.

Table 2: Coefficients of the 4-component model. Note, that the coefficient for the trend agrees within the uncertainty with the result found from the direct regression of the TSI and B_R values at the minima as shown in Fig. 13c.

S_Q	a_F	a_N	a_S	a_T	r^2
1364.66	76.17	122.91	-0.7997	0.3466	0.8444
standard error	1.02	0.73	0.0048	0.0032	

Earlier results of the two and three-component models (e.g. Fröhlich and Lean, 2004) showed that 77.2 % and 78.6 % of the variance are explained. The four-component model shown here explains 84.4 %, which is an important improvement over the 3-component model.

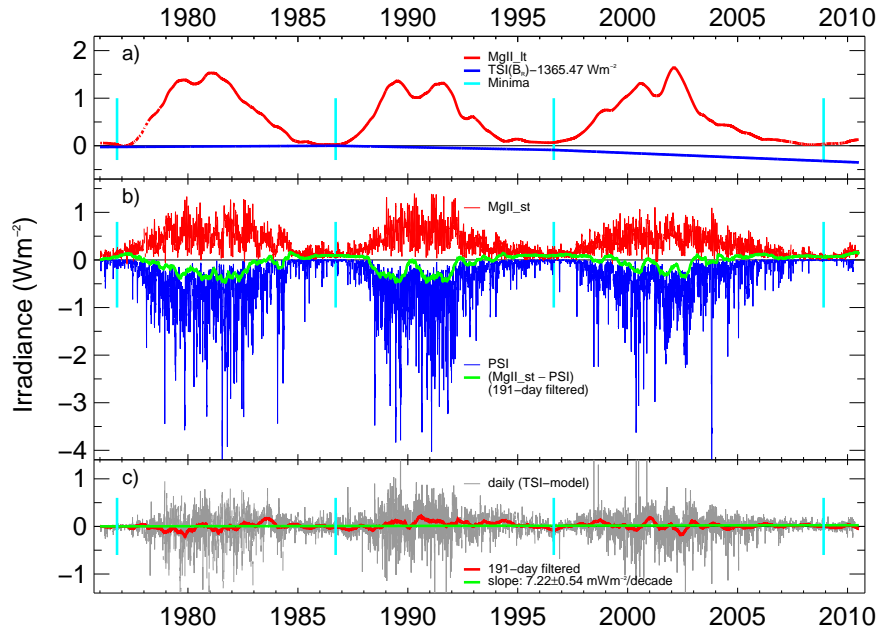


Figure 17: Panel a) shows the calibrated long-term (MgII-lt (red) together with the corresponding trend (blue) of the ‘quiet sun’, and panel b) the calibrated short-term (MgII-st (red) and PSI (blue). Note that all three panels have the same scale. The green curve of b) shows the 191-day filtered difference between facular and sunspot influence. The net effect of active regions increases TSI during minima by $\approx 0.08\text{Wm}^{-2}$, whereas during maxima TSI is dominated by sunspots and a decrease by $\approx 0.25\text{Wm}^{-2}$ is observed.

The trend is well represented by the model with a slope of the TSI- B_R relation of 0.3466 ± 0.0032 which is close to the result of direct correlation with 0.3357 ± 0.1426 (including the minimum value at 1977). That is within the correlation uncertainty and within $3-\sigma$ of the model coefficient uncertainty they agree. This confirms the need for the fourth component

which is related to the strength of the activity, and not to the manifestations of the surface magnetism. This is obviously in contradiction to the vastly accepted assumption that *all* the changes of TSI and SSI are due to surface magnetism. This means that the UV radiation has probably no long-term trend even back to the Maunder Minimum, only changes of the cycle amplitude. On the other hand TSI shows a long-term trend which could be due to a change of the temperature of the photosphere, which changes TSI but the UV radiation only by a very small amount (Tapping et al., 2007; Fröhlich, 2009b). As the strength of activity may also be represented by the total number of sunspots during a cycle, this can also be used to determine the long-term trend of TSI (see e.g. Lean et al., 1995; Wang et al., 2005). So, a long-term trend for TSI on top of the amplitude changes of the individual cycles is highly probable. But the same long-term trend cannot be applied to the UV irradiance, which then shows only the variation of the cycle amplitudes.

5 Importance of Continuing TSI Monitoring from Space

Observation of TSI during the last three solar cycles have revealed very interesting and partly unexpected variations which challenges the solar physics community. The differences between the behaviour of TSI during each cycle are an important test bed for proposed explanations and at present the variability can be explained to a high degree (nearly 85% of the variance during the last three cycles), although the understanding of the underlying mechanisms is still incomplete. The success of the 4-component proxy model proposed by Fröhlich (2010b) and the results presented here suggest two different mechanisms producing irradiance variability, which are both related to the strength of solar activity: (1) related to the manifestations of the surface magnetism during a cycle and (2) related to a global temperature change on longer time scales. This contradicts the assumption that *all* irradiance changes (total and spectral) are due to surface magnetism on solar cycle and secular time-scales (e.g. Solanki et al., 2005; Krivova et al., 2007; Lockwood, 2010), which provokes interesting discussions about the physical mechanisms on the sun. This controversy has fundamental consequences on the long-term behaviour of the UV radiation and needs certainly more analysis. Data from the ascending phase of the just-started solar cycle 24 will certainly deepen the understanding and provide new insights.

Although the understanding of TSI has well advanced during the last decades there is a need to continue the observations with overlapping missions. This is not only to continue the present TSI record, but also to learn more about the reliability of the understanding, which is ‘only’ based on three solar cycles. As for cycle 23, the next one may be different again and the understanding may have to be revised – a great opportunity for the advancement of understanding the solar engine.

Further Reading

This script is based on several papers - partly ‘in press’ or ‘in preparation’ (annotated by *), meaning that they are not yet citable and only presented for use together with this script. They can be downloaded from `ftp://ftp.pmodwrc.ch/pub/Claus/Alpbach2010/` as: `LectureNotes_CF.pdf` (this Script), `SolarConstant_subm.pdf` * (Fröhlich, 2010d), `Photons_from_Space_Ch32.pdf` * (Fröhlich, 2010a), `KyotoCAWSES_217_2009.pdf` (Fröhlich, 2009a), `A&ARev_12_273_2004.pdf` (Fröhlich and Lean, 2004) and `AA_501_27_2009.pdf` (Fröhlich, 2009b).

References

- C.G. Abbot. Periodicities in the solar-constant measures. *Smithsonian Misc.Coll.*, 117(10):1–31, 1952.
- C.G. Abbot. Solar variation and weather. *Smithsonian Misc.Coll.*, 146(3):1–62, 1963.
- L.B. Aldrich and W.H. Hoover. *Annals of the Astrophysical Observatory of the Smithsonian Institution*, volume 7, chapter 7: Statistical Studies of the Solar-Constant Record, pages 165–168. Smithsonian Institution, Washington, DC, U.S.A., 1954.

- L. A. Balmaceda, S. K. Solanki, N. A. Krivova, and S. Foster. A homogeneous database of sunspot areas covering more than 130 years. *J. Geophys. Res.*, 114:A07104, 2009. doi: 10.1029/2009JA014299.
- R. W. Brusa and C. Fröhlich. Absolute radiometers (PMO6) and their experimental characterization. *Appl. Opt.*, 25: 4173–4180, 1986.
- G. A. Chapman, A. M. Cookson, and J. J. Dobias. Variations in total solar irradiance during solar cycle 22. *J. Geophys. Res.*, 101:13541–13548, 1996.
- P. Charbonneau. Dynamo Models of the Solar Cycle. *Living Reviews in Solar Physics*, 2:2–83, 2005.
- D. Crommelynck, A. Fichot, R. B. Lee III, and J. Romero. First realisation of the space absolute radiometric reference (SARR) during the ATLAS 2 flight period. *Adv. Space Res.*, 16:(8)17–(8)23, 1995.
- D. A. Crommelynck, R. W. Brusa, and V. Domingo. Results of the solar constant experiment onboard Spacelab 1. *Sol. Phys.*, 107:1–9, 1987.
- S. Dewitte, D. Crommelynck, and A. Joukoff. Total solar irradiance observations from DIARAD/VIRGO. *J. Geophys. Res.*, 109:A02102, 2004a. doi: 10.1029/2002JA009694.
- S. Dewitte, D. Crommelynck, S. Mekaoui, and A. Joukoff. Measurement and Uncertainty of the Long-Term Total Solar Irradiance Trend. *Sol. Phys.*, 224:209–216, 2004b. doi: 10.1007/s11207-005-5698-7.
- J. A. Eddy. The maunder minimum. *Science*, 192:1189–1202, 1976.
- I. Ermolli, S. K. Solanki, A. G. Tlatov, N. A. Krivova, R. K. Ulrich, and J. Singh. Comparison among Ca II K Spectroheliogram Time Series with an Application to Solar Activity Studies. *Astrophys. J.*, 698:1000–1009, 2009. doi: 10.1088/0004-637X/698/2/1000.
- M. Fligge and S. K. Solanki. Inter-Cycle Variations of Solar Irradiance: Sunspot Areas as a Pointer. *Sol. Phys.*, 173: 427–439, 1997.
- P. Foukal, L. Bertello, W. Livingston, A. Pevtsov, J. Singh, A. Tlatov, and R. Ulrich. A century of solar Ca II K measurements and their implications for solar UV driving of climate. *Sol. Phys.*, 255:229–238, 2009. doi: 10.1007/s11207-009-9330-0.
- P. V. Foukal and J. Lean. Magnetic modulation of solar luminosity by photospheric activity. *Astrophys. J.*, 328:347–357, 1988.
- P. V. Foukal and J. Lean. An empirical model of total solar irradiance variation between 1874 and 1988. *Science*, 247: 556–558, 1990.
- C. Fröhlich. Observations of irradiance variability. *Space Sci. Rev.*, 94:15–24, 2000.
- C. Fröhlich. Long-term behaviour of space radiometers. *Metrologia*, 40:60–65, 2003.
- C. Fröhlich. Solar irradiance variability since 1978: Revision of the PMOD composite during solar cycle 21. *Space Sci. Rev.*, 125:53–65, 2006. doi: 10.1007/s11214-006-9046-5.
- C. Fröhlich. Total Solar Irradiance Variability: What have we learned about its Variability from the Record of the last three Solar Cycles? In T. Tsuda, R. Fujii, K. Shibata, and M. A. Geller, editors, *Climate and Weather of the Sun-Earth System(CAWSES): Selected Papers from the 2007 Kyoto Symposium*, pages 217–230. Terra Publishing, Setagaya-ku, Tokyo, Japan, 2009a. available at <http://www.terrapub.co.jp/onlineproceedings/ste/CAWSES2007/index.html>.
- C. Fröhlich. Evidence of a long-term trend in total solar irradiance. *Astron. Astrophys.*, 501:L27–L30, 2009b. doi: {10.1051/0004-6361/200912318}.
- C. Fröhlich. Solar radiometry. In M. C.E. Huber, J.L. Culhane, A. Pauluhn, J.G. Timothy, K. Wilhelm, and A. Zehnder, editors, *Observing Photons in Space*, ISSI Scientific Reports SR-009, chapter 32. ESA Publication Division, Noordwijk, The Netherlands, 2010a. in press.

- C. Fröhlich. A Four-Component Proxy Model of Total Solar Irradiance, calibrated during Solar Cycles 21–23. 2010b. in preparation.
- C. Fröhlich. Degradation of radiometers in space:an update, 2010c. Can be downloaded from <ftp://ftp.pmodwrc.ch/pub/Claus/Publications/Degrad04.pdf>.
- C. Fröhlich. *Solar Constant and Total Solar Irradiance Variations*. Springer Science-Business Media, LLC, 233 Spring Street, New York, NY 10013-1578, USA, 2010d. in preparation for Encyclopedia of Sustainability Science and Technology.
- C. Fröhlich and M. Anklin. Uncertainty of total solar irradiance: An assessment of the last 20 years of space radiometry. *Metrologia*, 37:387–391, 2000.
- C. Fröhlich and W. Finsterle. VIRGO radiometry and total solar irradiance 1996-2000 revised. In P. Brekke, B. Fleck, and J. B. Gurman, editors, *Recent Insights Into the Physics of the Sun and Heliosphere: Highlights from SOHO and Other Space Missions*, pages 105–110, San Francisco, USA, 2001. IAU Symposium, Vol. 203, ASP Conference Series.
- C. Fröhlich and J. Lean. Total solar irradiance variations: The construction of a composite and its comparison with models. In F. L. Deubner, J. Christensen-Dalsgaard, and D. Kurtz, editors, *IAU Symposium 185: New Eyes to See Inside the Sun and Stars*, pages 89–102, Dordrecht, The Netherlands, 1998a. Kluwer Academic Publ.
- C. Fröhlich and J. Lean. The sun’s total irradiance: Cycles and trends in the past two decades and associated climate change uncertainties. *Geophys. Res. Lett.*, 25:4377–4380, 1998b.
- C. Fröhlich and J. Lean. Solar radiative output and its variability: Evidence and mechanisms. *Astron. Astrophys. Rev.*, 12: 273–320, 2004. doi: 10.1007/s00159-004-0024-1.
- C. Fröhlich, J. Romero, H. Roth, C. Wehrli, B. N. Andersen, T. Appourchaux, V. Domingo, U. Telljohann, G. Berthomieu, P. Delache, J. Provost, T. Toutain, D. Crommelynck, A. Chevalier, A. Fichot, W. Däppen, D. O. Gough, T. Hoeksema, A. Jiménez, M. Gómez, J. Herreros, T. Roca Cortés, A. R. Jones, and J Pap. VIRGO: Experiment for helioseismology and solar irradiance monitoring. *Sol. Phys.*, 162:101–128, 1995.
- C. Fröhlich, D. Crommelynck, C. Wehrli, M. Anklin, S. Dewitte, A. Fichot, W. Finsterle, A. Jiménez, A. Chevalier, and H. J. Roth. In-flight performances of VIRGO solar irradiance instruments on SOHO. *Sol. Phys.*, 175:267–286, 1997.
- K. Harvey. Irradiance models based on solar magnetic field observations. In J. M. Pap, C. Fröhlich, H. S. Hudson, and S. K. Solanki), editors, *The Sun as a Variable Star: Solar and Stellar Irradiance Variations*, pages 217–225, Cambridge, UK, 1994. Cambridge University Press.
- K. Harvey. Solar Active Regions: Ephemeral. In P. Murdin, editor, *Encyclopedia of Astronomy and Astrophysics*, Encyclopedia of Astronomy and Astrophysics, pages 1–5. Institute of Physics Publishing, Bristol, U.K., 2000. doi: 10.1888/0333750888/2275. Article 2275.
- D. F. Heath and B. M. Schlesinger. The Mg-280nm doublet as a monitor of changes in solar ultraviolet irradiance. *J. Geophys. Res.*, 91:8672–8682, 1986.
- P. G. Judge and S. H. Saar. The Outer Solar Atmosphere during the Maunder Minimum: A Stellar Perspective. *Astrophys. J.*, 663:643–656, 2007. doi: 10.1086/513004.
- G. Kopp and G. Lawrence. The Total Irradiance Monitor (TIM): Instrument Design. *Sol. Phys.*, 230:91–109, 2005. doi: 10.1007/s11207-005-7446-4.
- G. Kopp, G. Lawrence, and G. Rottman. The Total Irradiance Monitor (TIM): Science Results. *Sol. Phys.*, 230:129–139, 2005. doi: 10.1007/s11207-005-7433-9.
- N. A. Krivova, S. K. Solanki, M. Fligge, and Y. C. Unruh. Reconstruction of solar total and spectral irradiance variations in cycle 23: is solar surface magnetism the cause? *Astron. Astrophys.*, 399:L1–L4, 2003.
- N. A. Krivova, L. Balmaceda, and S. K. Solanki. Reconstruction of solar total irradiance since 1700 from the surface magnetic flux. *Astron. Astrophys.*, 467:335–346, 2007. doi: 10.1051/0004-6361:20066725.

- N. A. Krivova, S. K. Solanki, and T. Wenzler. ACRIM-gap and total solar irradiance revisited: Is there a secular trend between 1986 and 1996? *Geophys. Res. Lett.*, 36:L20101, 2009. doi: 10.1029/2009GL040707.
- J. Lean, J. Beer, and R. Bradley. Reconstruction of solar irradiance since 1610: Implications for climate change. *Geophys. Res. Lett.*, 22:3195–3198, 1995.
- R. B. Lee III, M. A. Gibson, R. S. Wilson, and S. Thomas. Long-term total solar irradiance variability during sunspot cycle 22. *J. Geophys. Res.*, 100:1667–1675, 1995.
- W. Livingston and L. Wallace. The Sun’s immutable basal quiet atmosphere. *Sol. Phys.*, 212:227–237, 2003.
- M. Lockwood. Solar change and climate: An update in the light of the current exceptional solar minimum. *Proc. R. Soc. A*, 466:303–329, 2010. doi: 10.1098/rspa.2009.0519.
- M. Lockwood, M. Owens, and A. P. Rouillard. Excess open solar magnetic flux from satellite data: 1. Analysis of the third perihelion Ulysses pass. *J. Geophys. Res.*, 114:A11103, 2009a. doi: 10.1029/2009JA014449.
- M. Lockwood, M. Owens, and A. P. Rouillard. Excess open solar magnetic flux from satellite data: 2. A survey of kinematic effects. *J. Geophys. Res.*, 114:A11104, 2009b. doi: 10.1029/2009JA014450.
- A. Ortiz. Solar cycle evolution of the contrast of small photospheric magnetic elements. *Adv. Space Res.*, 35:350–360, 2005. doi: 10.1016/j.asr.2005.03.014.
- A.K. Pierce. Limb darkening. In A.N. Cox, editor, *Allen’s Astrophysical Quantities*, chapter 14.7, pages 355–357. The Althone Pree, Ltd, London, 2nd edition edition, 2nd edition, 2000.
- A. P. Rouillard, M. Lockwood, and I. Finch. Centennial changes in the solar wind speed and in the open solar flux. *J. Geophys. Res.*, 112:A05103, 2007. doi: 10.1029/2006JA012130.
- N. Scafetta. Climate Change and its Causes, a Discussion about some Key Issues. In *SPPI Original Paper*, pages 1–56. Science and Public Policy Institute, Haymarket, Va 20169, U.S.A., March, 18 2010. http://scienceandpublicpolicy.org/images/stories/papers/originals/climate_change_cause.pdf.
- N. Scafetta and R. C. Willson. ACRIM-gap and TSI trend issue resolved using a surface magnetic flux TSI proxy model. *Geophys. Res. Lett.*, 36:L05701, 2009. doi: 10.1029/2008GL036307.
- S. K. Solanki, N. A. Krivova, and T. Wenzler. Irradiance models. *Adv. Space Res.*, 35:376–383, 2005. doi: 10.1016/j.asr.2004.12.077.
- M. Steinegger, P. N. Brandt, J. Pap, and W. Schmidt. Sunspot photometry and the total solar irradiance deficit measured in 1980 by ACRIM. *Astrophys. Space Sci.*, 170:127–133, 1990.
- M. Steinegger, M. Vazquez, J. A. Bonet, and P. N. Brandt. On the Energy Balance of Solar Active Regions. *Astrophys. J.*, 461:478–498, 1996. doi: 10.1086/177075.
- F. Steinhilber, J. A. Abreu, and J. Beer. Solar modulation during the Holocene. *Astrophys. Space Sci. Trans.*, 4:1–6, 2008.
- F. Steinhilber, J. Beer, and C. Fröhlich. Total solar irradiance during the holocene. *Geophys. Res. Lett.*, 36:L19704, 2009. doi: {10.1029/2009GL040142,}.
- K. F. Tapping, D. Boteler, P. Charbonneau, A. Crouch, A. Manson, and H. Paquette. Solar Magnetic Activity and Total Irradiance Since the Maunder Minimum. *Sol. Phys.*, 246:309–326, 2007. doi: 10.1007/s11207-007-9047-x.
- A. G. Tlatov, A. A. Pevtsov, and J. Singh. A New Method of Calibration of Photographic Plates from Three Historic Data Sets. *Sol. Phys.*, 255:239–251, 2009. doi: 10.1007/s11207-009-9326-9.
- Y. C. Unruh, S. K. Solanki, and M. Fligge. Modelling solar irradiance variations: Comparison with observations, including line-ratio variations. *Space Sci. Rev.*, 94:145–152, 2000.

- R. A. Viereck and M. Snow. Update of the composite Mg II index. personal communication; a weekly updated version is available from <http://lasp.colorado.edu/lisird/mgii/mgii.html>, 2008.
- Y.-M. Wang, J. L. Lean, and N. R. Sheeley. Modeling the Sun's Magnetic Field and Irradiance since 1713. *Astrophys. J.*, 625:522–538, 2005. doi: 10.1086/429689.
- T. Wenzler. *Reconstruction of Solar Irradiance Variations in Cycles 21-23 based on Surface Magnetic Fields*. PhD thesis, ETH Nr 16199, Eidgenössische Technische Hochschule, Zürich, 2005.
- T. Wenzler, S. K. Solanki, and N. A. Krivova. Reconstructed and measured total solar irradiance: Is there a secular trend between 1978 and 2003? *Geophys. Res. Lett.*, 36:L11102, 2009. doi: 10.1029/2009GL037519.
- R. C. Willson. Active cavity radiometer type iv. *Appl. Opt.*, 18:179–188, 1979.
- R. C. Willson. Total solar irradiance trend during solar cycles 21 and 22. *Science*, 277:1963–1965, 1997. see also comment by R.Kerr on page 1923 of the same issue of Science.
- R. C. Willson. The ACRIMSAT/ACRIM III Experiment: Extending the Precision, Long-Term Total Solar Irradiance Climate Database. *THE EARTH OBSERVER*, 13:14–17, 2001.
- R. C. Willson and H. S. Hudson. The Sun's luminosity over a complete solar cycle. *Nature*, 351:42–44, 1991.
- R. C. Willson and A. V. Mordvinov. Secular Total Solar Irradiance trend during solar cycles 21-23. *Geophys. Res. Lett.*, 30:1199, 2003. doi: 10.1029/2002GL016038.
- R. C. Willson, S. Gulikis, M. Janssen, H. S. Hudson, and G. A. Chapman. Observations of solar irradiance variability. *Science*, 211:700–702, 1981.
- R.C. Willson and R.S. Helizon. Active cavity radiometer irradiance monitors: S.I. measurements uncertainties. presented at the "Total Solar Irradiance Workshop" at NIST, Gaithersberg, Md, USA, 18-20 July 2005, 2005.
- T. N. Woods, W. K. Tobiska, G. J. Rottman, and J. R. Worden. Improved solar Lyman α irradiance modeling from 1947 through 1999 based on UARS observations. *J. Geophys. Res.*, 105:27195–27216, 2000. doi: 10.1029/2000JA000051.